Imaging multilayered objects with complex geometry

Tomasz LUKOMSKI [1], Tadeusz STEPINSKI [1]
[1] AGH University of Science and Technology, Krakow, Poland
Contact e-mail: - lukomski@agh.edu.pl

Abstract. Imaging of solid layered objects using ultrasound presents normally a difficult task. Delay-and-sum (DAS) method, a standard and well-known method used for improving resolution in immersion setup, cannot properly reconstruct an image of layered objects. More advanced algorithms have been proposed for that purpose, like multi layered delay-and-sum (MLDAS) and ray tracing or phase shift migration (PSM). However, these algorithms work properly only when layers are parallel to each other and their surface is perpendicular to the transducer's axis. When an object has complex geometry the problem is even more complicated and only one of those algorithms (ray tracing) is capable of reconstructing the ultrasound image properly.

In this paper two algorithms capable of imaging layered objects with complex geometry are presented and their performance is compared: first, is the modified MLDAS that takes under consideration object geometry, and second, the generalized version of PSM (GPSM). The Matlab implementations of those algorithms are evaluated on the experimental data from a copper block immersed in water. The results are compared and advantages and disadvantages of the presented methods are discussed. Half power resolution and signal-to-noise ratio are measured and presented as a quality indicator. Additionally, some modifications to the GPSM algorithm are presented that can enhance the reconstructed image quality.

1. Introduction

In the 20th century the advancement in ultrasound signal processing has enabled easy access to high quality images of objects interior, allowing better evaluation and quality assessment. In non-destructive testing (NDT) ultrasounds are very common, however, more advanced imaging algorithms are not very well known in industry. One of the oldest and most popular algorithms Delay-and-Sum (DAS) is only applicable in simple cases where only one layer is taken under consideration [1]. When it comes to problems where more than one layer is inspected, then other algorithms should be taken under consideration. One of the most obvious choices is to use the ray-tracing algorithm. That can take under consideration multiple layers and even the sample geometry [2]. However, there are other solutions that might give similar results, but might be easier for implementations or faster or even give better results.

In this paper two algorithms are presented that allow imaging multilayered objects and taking under consideration their geometry. The first one is improved Multi Layer Delay-and-Sum (MLDAS) [3, 4]. The simple MLDAS takes under consideration only layered objects that are parallel to the transducer movement. Algorithm presented here

introduces some changes that allow the algorithm to take under consideration the geometry of the sample within certain limits.

The second algorithm called Generalized Phased Shift Migration (GPSM) is implemented in the frequency domain. The computation is based on the seismography algorithm developed by Gazdag in [5, 6]. The algorithm was also introduced in NDT in multiple variations in [7, 8, 9]. The algorithm allows computation in an efficient way using the Fourier transform. Moreover, it also takes object geometry under consideration. In the paper a modification to a signal pre-processing step is introduced that results in enhanced reconstructed image.

The paper compares these two algorithms with each other in manner of lateral resolution, signal-to-noise ratio (SNR) and evaluation time of those algorithms implemented in Matlab.

2. Theory

In this section a brief description of presented algorithms is provided. The first part concentrates on multi layered delay-and-sum algorithm, followed by the generalized phased shift migration method.

1.1 MLDAS

In a conventional DAS algorithm for a single layer object, the delay time is calculated as:

$$t(x-x',z) = \frac{2}{c} \cdot \sqrt{(x-x')^2 + (z-Z)^2} \tag{1}$$

For multilayered object the time cannot be calculated with this equation. At every layer interface there is a reflection and refraction affect that makes the wave path irregular. What is more, every path has different wave velocity. Knowing the incident angle of a wave at the interface, the refracted wave can be calculated using Snell's law. However, it is impossible to calculate exact wave path analytically [10]. For this problem a numerical ray-tracing can be employed [2, 10, 11]. Here, an approximate solution is given, often used in processing of seismic data [3].The solution is based on the concept of root-mean-square (RMS) velocity. Comparison of wave paths for DAS and MLDAS are presented in figure 1(a) and 1(b).

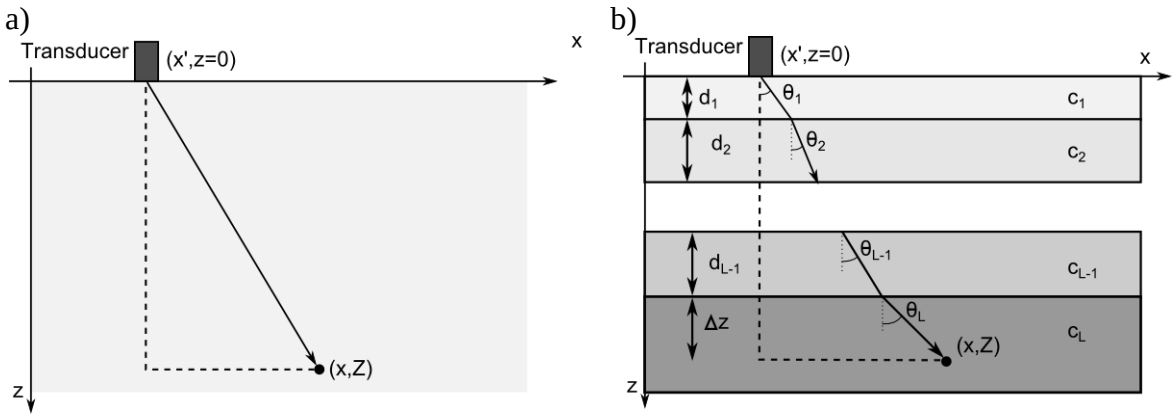

Fig. 1. Wave path in standard DAS (a) and MLDAS (b)

The velocity c is assumed to be the function that changes with depth $c(z)$. The one-way travel time for a pulse following a vertical path from Z to z can be written as:

$$\tau(z) = \sum_{l=1}^{L-1} \frac{d_l}{c_l} + \frac{\Delta z}{c_L} \tag{2}$$

thus the wave velocity can also be expressed as a function of τ , $c(\tau)$. The RMS velocity is the root-mean-square velocity with respect to τ,

$$c_{rms} = \sqrt{\frac{\sum_{l=1}^{L-1} c_l \cdot d_l + c_L \cdot \Delta z}{\tau(z)}} \tag{3}$$

Expressing the one-way delay time between transducer and scatterer as Taylor series:

$$t^2(x - x', z) = \tau^2 \cdot (z) + a_2 \cdot (x - x')^2 + a_4 \cdot (x - x')^4 + \cdots \tag{4}$$

where only even terms are included due to symmetry. Omitting all higher order terms and using the coefficient $a_2 = 1/c_{rms}^2(z)$ [3], we obtain an expression for the travel time which is approximate but accurate for small offsets $(x - x')$:

$$t_{rms}(x - x', z) = 2 \cdot \sqrt{\tau^2(z) + \frac{(x - x')^2}{c_{rms}^2(z)}} \tag{5}$$

The focused image pixel $i_p(x, z)$ is then given by:

$$i_p(x, z) = \int \alpha(\hat{x}) \cdot s(t_{rms}(x - x', z), x') dx' \tag{6}$$

where $\alpha(\hat{x})$ denotes general apodization weights. For rectangular window:

$$\alpha(\hat{x}) = \begin{cases} 1, & |\hat{x}| < 1/2 \\ 0, & otherwise \end{cases} \tag{7}$$

where:

$$\hat{x} = \frac{x - x'}{\Delta x(z)} \tag{8}$$

The divergent angle $\theta_l$can be calculated with:

$$\theta_l = sin^{-1}\left(\frac{c_l}{c_1} \cdot \sin(\Delta\theta/2)\right) \tag{9}$$

Due to the fact that beam spread increases with depth it can be calculated as:

$$\Delta x = 2 \cdot \left(\sum_{l=1}^{L-1} d_l \cdot \tan(\theta_l) + \Delta z \cdot \tan(\theta_L)\right) \tag{10}$$

1.2 MLDAS for velocity model

The improvement in the MLDAS algorithm is not big; however, it gives the necessary information about the geometry for the calculations. The basic assumption is to calculate the root mean square value of the layer dimension in depth, and root mean square value of the pixel depth in a specific layer. The calculation of those values is described as:

$$d_l = \sqrt{\frac{d_l^2(x') + d_l^2(x)}{2}} \tag{11}$$

and

$$\Delta z = \sqrt{\frac{\Delta z(x') + \Delta z(x)}{2}} \tag{12}$$

In figure 2 the calculation schematic for the specific pixel is presented.

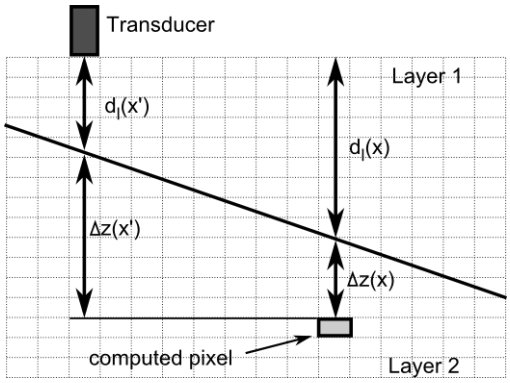

Fig. 2. Visual representation of the improved MLDAS concept

For more complex geometries the number of points between x' and x can be increased. This assumption introduces an error in calculations. The larger the distance between the transducer and computed pixel is, the greater the error is. However, using apodization as presented in section 2.1 reduces this effect. It can be seen in section 3.2 that the reconstructed image has fairly good quality.

2.3 Generalized Phased Shift Migration

The GPSM algorithm is derived from the wave equation. Full derivation can be found in based on [6, 12]. In this paper only the basic algorithm flow is presented figure 3.

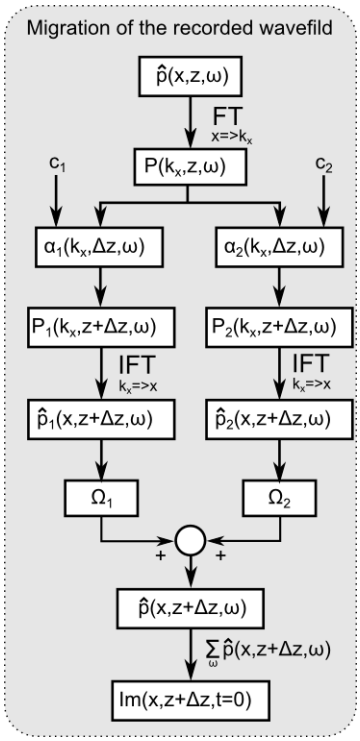

Fig. 3. The computational diagram for the GPSM algorithm.

Notation FT and IFT in the figure is Fourier Transform and Inverse Fourier Transform, respectively.

The algorithm computes the data in the frequency domain, therefore the pressure recorded at depth $z = 0$ must be transformed using the double Fourier transform.

$$P(k_x, z = 0, \omega) = FT_{x=>k_x} FT_{t=>\omega}[p(x, z = 0, t)] \tag{13}$$

The phase shift factor $\alpha(\mathrm{k_x}, \mathrm{z}, \omega)$ is responsible for the data migration from depth $z = 0$ to any depth z.

$$P(k_x, z, \omega) = P(k_x, z = 0, \omega) \cdot \alpha(\mathrm{k_x}, \mathrm{z}, \omega) \tag{14}$$

where $\alpha(\cdot)$ is written as:

$$\alpha(k_x, z, \omega) = \exp\left(-jz\sqrt{\frac{\omega^2}{4c^2} + k_x^2}\right) \tag{15}$$

1.3 Windowed Generalized Phased Shift Migration

The basic GPSM algorithm is gives very good results, what is presented in section 3.2. However, due to the frequency domain implementation the algorithm suffers from some numerical noise that influences, to some extent, the final image quality. To reduce this unwanted effect some pre-processing is required. Firstly the velocity model used for calculation should be smoothed. The sharp transition between two mediums, like water-copper boundary, is sharp and sudden. The velocity change is from 1480 to 4760 m/s (Fig. 4 (a)). To reduce the negative effect of discontinuity in the model, the transition can be smoothed (Fig. 4(b)). However, one should have in mind that this operation slows down the computation process.

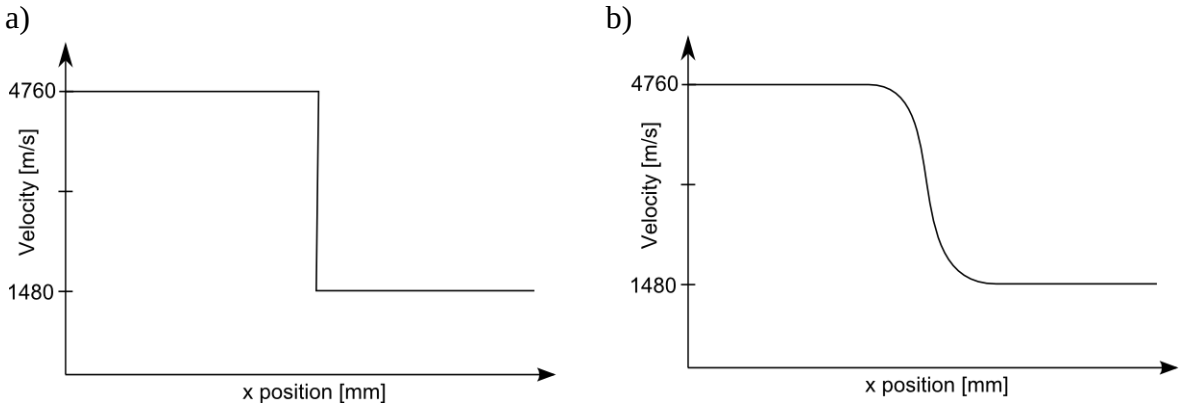

Fig. 4. An example velocity profile at depth z, real (a), smoothed (b)

Another pre-processing step can be done to the recorded signal. For every recorded signal at the specific time step/depth, the signal should be windowed in x dimension in respect to the velocity model. One can use different types of windowing functions like: Gaussian, Hamming, Hann etc. This operation doesn't slow down the algorithm itself, however requires some time before the main calculations.

Both of those pre-processing operation guarantees that the signal transformed from x to k_x domain will not suffer from discontinuities. Hence, the image quality should improve.

3. Experiment

In this section the setup of the performed experiment is presented, and results are shown. For comparison of the described algorithms reconstructed images are provided. Moreover, the SNR, half power lateral resolution is presented, and calculation times are given.

3.1 Experiment setup

To test the MLDAS algorithm and compare it with GPSM algorithm an experiment was performed. A copper block with artificial defects (side drilled holes) was placed in a water tank and tilted 5.6^o in respect to the transducer's movement axis. Each SDH was 1mm in diameter. The total number of defects was 18; however, the scanning area was limited to detect only 16 of them. The setup is presented in Fig. 5. The signal was acquired by a planar circular single transducer with parameters as presented in Table 1. A computerized test system, equipped with the ultrasonic board USPC3100LA from Socomate International, France, was used for data acquisition in the tests. The USPC board was controlled by National Instruments LabVIEW graphic user interface. Its sampling frequency was set to 50MHz and the spatial sampling step for B-scan acquisition was Δx = 0.5mm. The value of the sound velocity used in processing was set to c_{water} = 1480 m/s and c_{copper} = 4760 m/s. For the MLDAS post-processing and the GPSM algorithm a spatial sampling step in the z dimension (depth) was set to Δz = 0.2mm.

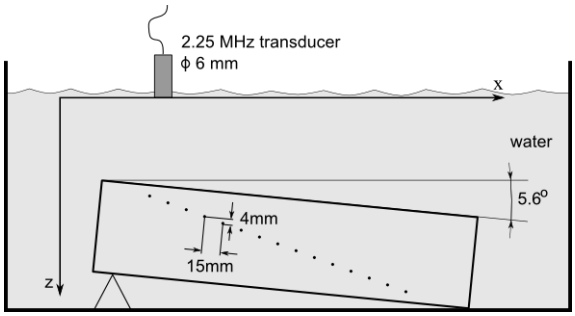

Fig. 5. Experiment setup with tilted copper block

Table 1. Transducer's parameters used in the experiment

Property name	Value
Diameter d [mm]	6.35
Central frequency f [MHz]	2.25
Producer	Panametrics

3.2 Experiment results

Recorded raw data for the tilted copper block is presented in Fig. 6(a). The image reconstructed with a standard DAS algorithm without taking under consideration layers and geometry is presented in Fig. 6(b). Only wave velocity in water is taken under consideration. A standard MLDAS is presented in figure 6(c), for calculation two layers were used (water and copper) the transition between layers was set as marked with the dashed line in the image. In figure 6(d) the MLDAS for a tilted velocity model is presented.

a)

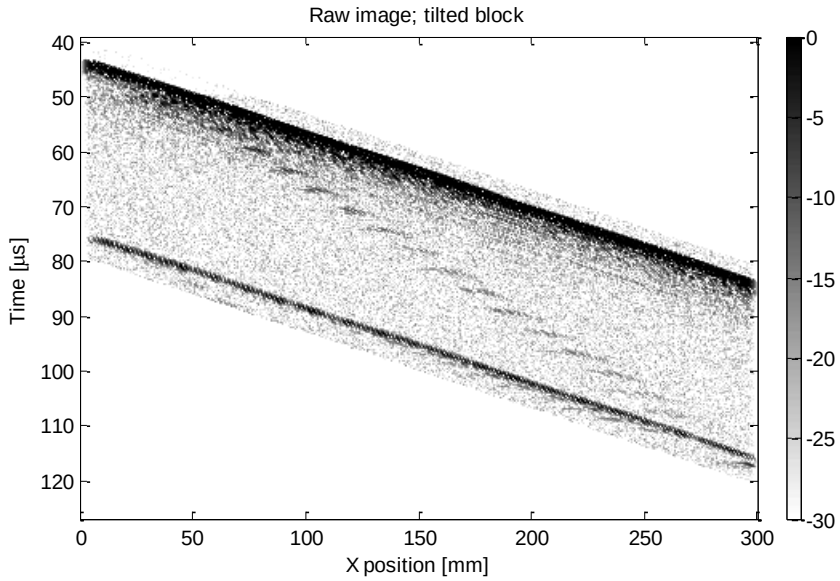
Raw image; tilted block
Time [µs]
X position [mm]
40
50
60
70
80
90
100
110
120
0
50
100
150
200
250
300
0
-5
-10
-15
-20
-25
-30

b)

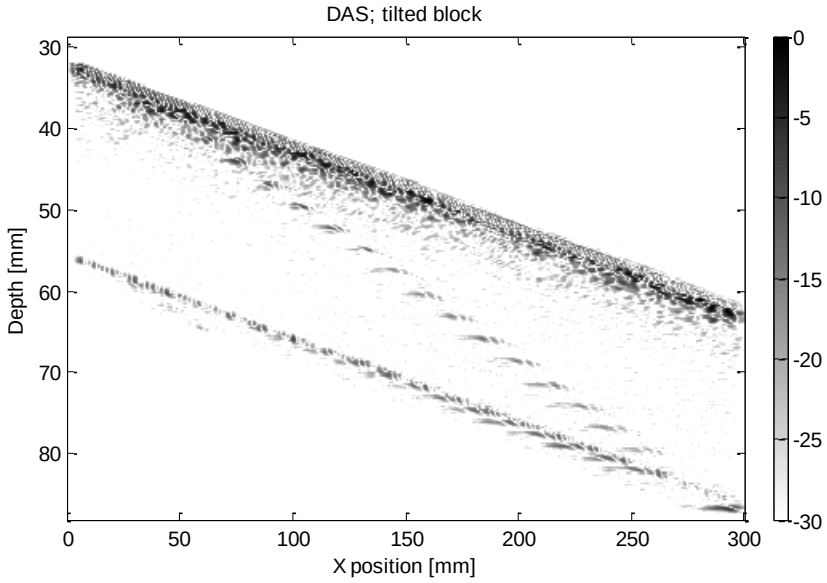
DAS; tilted block
Depth [mm]
X position [mm]
30
40
50
60
70
80
0
50
100
150
200
250
300
0
-5
-10
-15
-20
-25
-30

c)

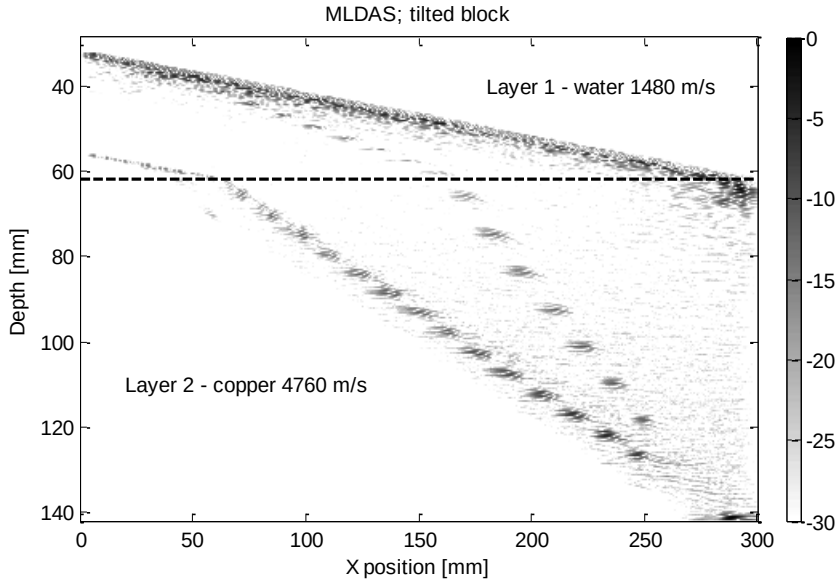
MLDAS; tilted block
Layer 1 - water 1480 m/s
Layer 2 - copper 4760 m/s
Depth [mm]
X position [mm]
40
60
80
100
120
140
0
50
100
150
200
250
300
0
-5
-10
-15
-20
-25
-30

d)

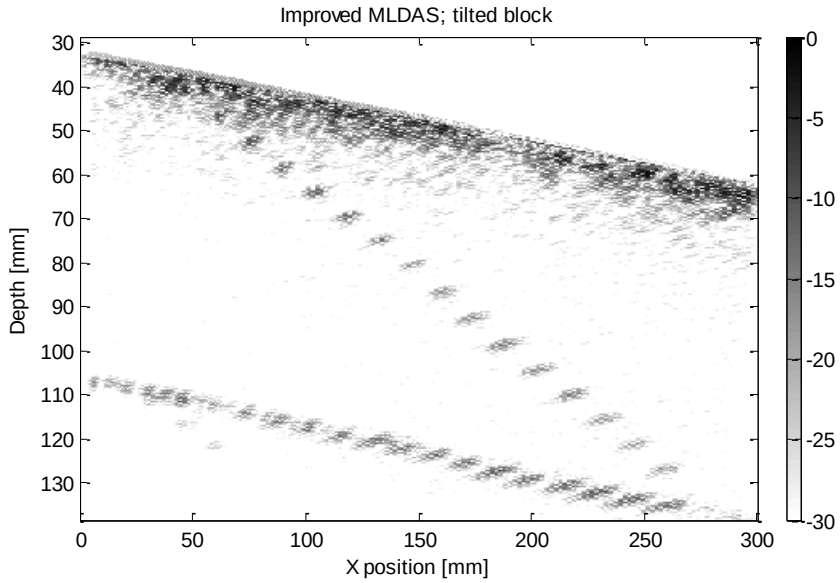

Fig. 6. Experiment data: unprocessed image (a), simple DAS processing (b), standard MLDAS (c) and improved MLDAS (d)

It is evident that without taking under consideration layers and geometry, the results are not satisfactory. Moreover, the simple MLDAS gives image with deformed object. For simple DAS and MLDAS the geometry of the tested sample and position of flaws are incorrectly calculated. The improved MLDAS gives good results, the geometry is properly reconstructed and flaws are visible at their actual positions with constant lateral resolution that is independent of depth.

In comparison, the results from the GPSM algorithm are presented in figure 7(a). The results are even better than the improved MLDAS. However, these results might also be improved by applying windowing function during the calculations. The improved image is visible in figure 7(b). At first the difference is not clearly visible, but in the comparison of SNR the difference is visible.

a)

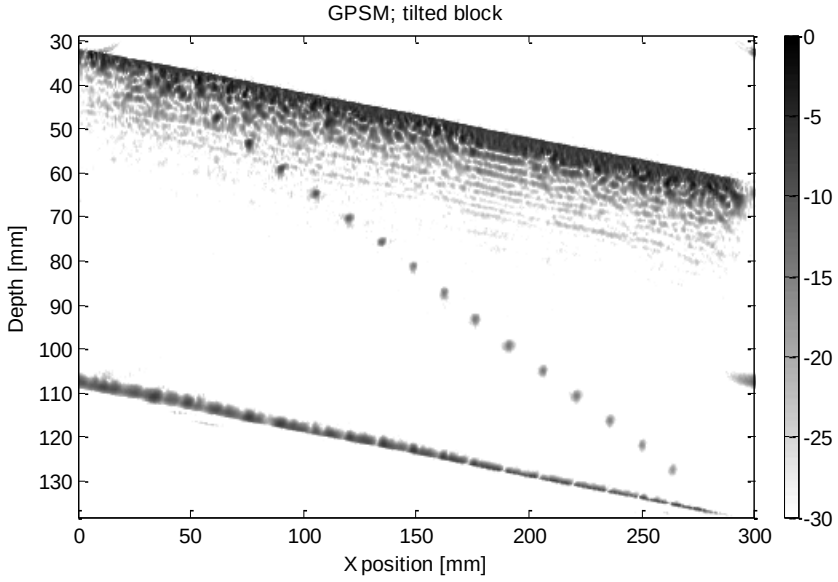

b)

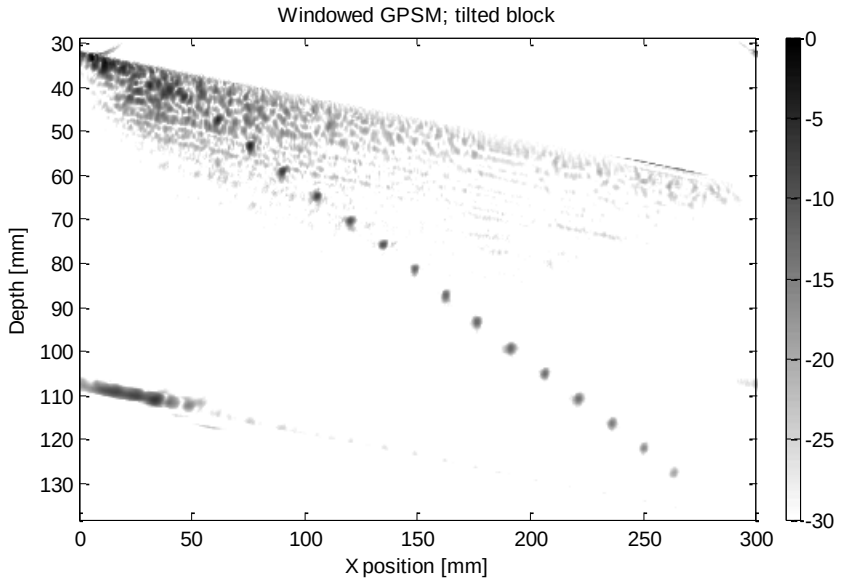

Fig. 7. Results for migration algorithms: standard GPSM (a), windowed GPSM (b)

In the Table 1 a comparison of SNR for different algorithms is presented. As can be seen All of the algorithms increase signal to noise ratio, however the windowed GPSM gives the best results.

Table 2. Signal-to-noise ration calculated from the images for selected SDHs

SNR of the signal in the images [dB]					
SDH no	Depth [mm]	Raw image SNR	MLDAS SNR	GPSM SNR	Windowed GPSM SNR
3	63	5.2	11.6	12.0	12.7
9	81	3.4	9.4	19.4	22.2
15	137	3.9	9.8	15.0	26.1

In Table 3 a comparison of the half power lateral resolution for the selected defects is presented. Holes no. 9 and 15 were impossible to measure due to the high noise level. Implemented algorithms were able to increase the lateral resolution. The migration algorithm in this case also gives better results than improved MLDAS, however, the algorithm implementation is more complex in case of GPSM. The windowing had no effect on the resolution.

Table 3. Half power resolution (HPR) of the selected SDHs

Half power lateral resolution of the selected SDH [mm]					
SDH no	Depth [mm]	HPR Raw	MLDAS HPR	GPSM HPR	Windowed GPSM HPR
3	63	10.9	7.0	3.1	3.0
9	81	unmeasurable	11.6	3.2	3.1
15	137	unmeasurable	10.7	3.0	3.1

In Table 4 an evaluation time is presented. The calculations were performed in Matlab on a laptop with a processor Intel core-i5 430M with 4GB RAM.

Table 4. Calculation time in Matlab

Algorithm	Calculation time
Improved MLDAS	Over 4000s
Standard GPSM	600s
Windowed GPSM	1300s

Time comparison is not very precise at this moment. All algorithms are implemented in a simple way to prove their functionality. However, the code was not optimised in any way.

4. Conclusions

This paper presents an improved MLDAS algorithm that can take under consideration an object's geometry. The SNR and the half power lateral resolution were presented to compare the differences between the image reconstruction algorithms. Due to some simplifications the results of the improved MLDAS are fair, but the GPSM algorithm shows better results. Additionally GPSM algorithm can be enhanced by some additional pre-processing (windowing and smoothing of the velocity model). This enhancement gives better SNR, but extends the computational time.

Comparison of the evaluation time in Matlab showed that simple GPSM is the fastest. However, this parameter might be different with properly implemented algorithm in GPGPU.

The paper lacks comparison with popular ray-tracing. However, the results might be similar to those obtained by GPSM with comparable evaluation time.

Acknowledgements

The authors would like to thank the AGH – University of Science and Technology for the provided support.

References

[1] S. R. Doctore, T. E. Hall and L. D. Reid, "SAFT - the evolution of a signal processing for ultrasonic testing," *NDT International,* vol. 19, no. 3, pp. 163-167, June 1986.

[2] A. Shlivinski and K. Langenberg, "Defect imaging with elastic waves in inhomogeneous{anisotropic materials with composite geometries.," *Ultrasonics,* vol. 46, no. 1, pp. 89-104, 2007.

[3] W. A. Schneider, "The common depth point stack.," *Proceedings of the IEEE,* vol. 72, no. 10, pp. 1330-1339, 1984.

[4] M. H. Skjelvareid and Y. Birkelund, "Ultrasound imaging using," *ASME 2010 Pressure Vessels and,* vol. 5, pp. 379-387, 2010.

[5] J. Gazdag, "Wave equation migration with the phase-shift method.," *Geophysics,* vol. 43, no. 7, p. 1342{1351, 1978.

[6] J. Gazdag and P. Sguazzero, "Migration of seismic data by phase shift plus interpolation.," *Geophysics,* vol. 49, no. 2, pp. 124-131, 1984.

[7] T. Olofsson, “Phase shift migration for imaging layered objects and objects immersed in water.,” *IEEE Trans. Ultrason., Ferroelectr., Freq. Control,* vol. 57, no. 11, pp. 2522-2530, 2010.

[8] K. Qin, C. Yang and F. Sun, “ Generalized frequency-domain synthetic aperture focusing technique for ultrasonic imaging of irregularly layered objects,” *IEEE Trans. Ultrason., Ferroelectr., Freq. Control* , vol. 61, no. 1, pp. 133 - 146 , 2014.

[9] T. Lukomski, “Non-stationary Phase Shift Migration for flaw detection in objects with lateral velocity variations,” *Insight, The Journal of The British Institute of Non-Destructive Testing,* vol. 56, no. 9, pp. 477-482, 2014.

[10] G. M. Margrave, “Numerical Methods in Exploration Seismology - with algorithms in Matlab.,”11 July 2003.
Available: http://www.crewes.org/ResearchLinks/FreeSoftware/NumMeth.pdf. [Accessed 20.2.2015].

[11] J. Johnson and B. and Barna, “The effects of surface mapping corrections with synthetic-aperture focusing techniques on ultrasonic imaging.,” *IEEE Transactions on Sonics and Ultrasonics,* vol. 30, no. 5, pp. 283-294, 1983.

[12] E. G. Williams, Fourier Acoustics: Sound Radiation and Nearfield Acoustical Holography, Academic Press, 1999.